Guided Wave Optics Laboratory

Report No. 67

Evaluation of Defect-Related Diffusion in Semiconductors by Electrooptical Sampling

Paul Biernacki, Henry Lee, and Alan R. Mickelson

February 15, 1995

Department of Electrical and Computer Engineering

University of Colorado at Boulder
Boulder, Colorado

unclassified
SECURITY CLASSIFICATION OF THIS PAGE

REPORT DOCUMENTATION PAGE

Form Approved OMB No. 0704-0188

1a. REPORT SECURITY CLASSIFICATION: unclassified	1b. RESTRICTIVE MARKINGS: none
2a. SECURITY CLASSIFICATION AUTHORITY: ~~DISCASS~~	3. DISTRIBUTION/AVAILABILITY OF REPORT: unrestricted
2b. DECLASSIFICATION/DOWNGRADING SCHEDULE: N/A	
4. PERFORMING ORGANIZATION REPORT NUMBER(S): ECE/GWOL/67	5. MONITORING ORGANIZATION REPORT NUMBER(S): DOD-ONRN00014-92-J-1190
6a. NAME OF PERFORMING ORGANIZATION: University of Colorado; 6b. OFFICE SYMBOL (If applicable):	7a. NAME OF MONITORING ORGANIZATION: Office of Naval Research, Attn: Dr. Arthur Jordan, Code 1114 SE
6c. ADDRESS (City, State, and ZIP Code): Electrical & Computer Engineering Dept., Boulder, CO 80309-0425	7b. ADDRESS (City, State, and ZIP Code): 800 N. Quincy Avenue, Arlington, VA 22217-5000
8a. NAME OF FUNDING/SPONSORING ORGANIZATION: Office of Naval Research; 8b. OFFICE SYMBOL (If applicable):	9. PROCUREMENT INSTRUMENT IDENTIFICATION NUMBER:
8c. ADDRESS (City, State, and ZIP Code): 800 N. Quincy Avenue, Arlington, VA 22217-5000	10. SOURCE OF FUNDING NUMBERS: PROGRAM ELEMENT NO. / PROJECT NO. / TASK NO / WORK UNIT ACCESSION NO.

11. TITLE (Include Security Classification)

(u) Evaluation of Defect Related Diffusion in Semiconductors by Electrooptical Sampling

12. PERSONAL AUTHOR(S): Paul Biernacki, Henry Lee, and Alan R. Mickelson

13a. TYPE OF REPORT	13b. TIME COVERED	14. DATE OF REPORT (Year, Month, Day)	15. PAGE COUNT
Manuscript	FROM _____ TO _____	2/15/95	39

16. SUPPLEMENTARY NOTATION

17. COSATI CODES			18. SUBJECT TERMS (Continue on reverse if necessary and identify by block number)
FIELD	GROUP	SUB-GROUP	

19. ABSTRACT (Continue on reverse if necessary and identify by block number)

The electrooptical sampling technique is used to assess the electrical behavior of ohmic contact regions in GaAs. For purpose, unique ohmic contact coplanar waveguides were fabricated and tested. A reduced electrooptical sampling signal is detected in certain ohmic contact regions. Since the electrical fields present in this device are known a priori, the deviation of the electrooptical signal from its nominal value is attributed to a deviation in the electrooptical coefficient. Defects introduced during the annealing step of the ohmic contact accelerated by existing dislocations are discussed as a mechanism capable of disrupting the electrooptic coefficient. A simple phenomenological diffusion model is presented to explain the mechanism responsible for the nulling of the electrooptical coefficient.

20. DISTRIBUTION/AVAILABILITY OF ABSTRACT	21. ABSTRACT SECURITY CLASSIFICATION
■ UNCLASSIFIED/UNLIMITED ☐ SAME AS RPT. ☐ DTIC USERS	unclassified
22a. NAME OF RESPONSIBLE INDIVIDUAL: Alan R. Mickelson	22b. TELEPHONE (Include Area Code): 303/492-7539; 22c. OFFICE SYMBOL:

DD Form 1473, JUN 86 — Previous editions are obsolete. — SECURITY CLASSIFICATION OF THIS PAGE

Report No. 67

Evaluation of Defect-Related Diffusion in Semiconductors by Electrooptical Sampling

Paul Biernacki, Henry Lee, and Alan R. Mickelson

February 15, 1995

Guided Wave Optics Laboratory
Department of Electrical and Computer Engineering
University of Colorado at Boulder
Boulder, Colorado 80309-0425

This work was supported by the Office of Naval Research under Contract #N00014-92-J-1190 and the Army Research Office under Contract #DAAL-03-92-G-0289.

Evaluation of Defect Related Diffusion in Semiconductors by Electrooptical Sampling

Paul Biernacki, Henry Lee, and Alan R. Mickelson

Department of Electrical & Computer Engineering,
University of Colorado
Boulder, Colorado 80309-0425

ABSTRACT

The electrooptical sampling technique is used to assess the electrical behavior of Ohmic contact regions in GaAs. For this purpose unique Ohmic contact coplanar waveguides were fabricated and tested. A reduced electrooptical sampling signal is detected in certain Ohmic contact regions. Since the electrical fields present in this device are known a priori, the deviation of the electrooptical signal from its nominal value is attributed to a deviation in the electrooptical coefficient. Defects introduced during the annealing step of the Ohmic contact accelerated by existing dislocations are discussed as a mechanism capable of disrupting the electrooptic coefficient. A simple phenomenological diffusion model is presented to explain the mechanism responsible for the nulling of the electrooptical coefficient.

I. INTRODUCTION

There have been many techniques employed to observe semiconductor defects. Among these techniques are laser scanning, laser scanning tomography, catholuminescence, photoluminescence, x-ray topography, and many variations of these methods [1-6]. The goal of defect recognition is not only to circumvent processing of a seriously defective substrate, but to also determine what seriously defective means. An open question is how do defects influence semiconductor properties and how can their deleterious effects be minimized. To answer these questions, one must know how accurately these defects can be observed, what effects they manifest on the semiconductor properties, and of course, how expensive it will be to minimize certain defects through heat cycling etc.

Defects will affect device performance. In particular, there have been studies demonstrating the correlation between defects present in the wafer and their influence on device performance. A correlation between microprecipitates and the side gating effect (or crosstalk perturbations) on field effect transistors (FET's) has been studied [7], [8]. This study indicated that small microprecipitates and dislocations can be observed and that their presence directly influences device behavior. Other studies revealed that dislocations in GaAs wafers have been found to influence the threshold voltage of FET's [9] and affect the sheet carrier concentration [10].

Defects are always present in the bulk grown process regardless of process used for growth (LEC etc.). Recently it has been shown that "memory" of defects exists in epi-layers grown on the substrate [11]. That is, regions with high defect density in the substrate will cause regions grown above these regions to also exhibit high defect densities. An important feature of defect rich crystal regions is that diffusion can occur rapidly through these defect sites [12]. Therefore, if dislocations or other defects are present in the substrate, subsequent processing steps in epitaxial regions above the defect regions could be affected. This will be especially true in the fabrication of an Ohmic contact. The diffusion profile below the electrode occurring during this processing step can be affected by existing dislocations and defects present in the substrate. Metals used in the formation of the Ohmic region can be diffused to much greater than expected depths, therefore, during the annealing process. Indeed, Fillard [12] has shown that their is a rapid variation in the diffusion profile below an Ohmic contact and that a significant defect density of microprecipitates has been found as deep as 10 μm below the contact with a density of 10^{16} to 10^{18} cm^{-3}.

Electrooptic sampling can be used to noninvasively sample the in situ electrical fields of a variety of monolithic microwave integrated circuits (MMIC's) [13-17]. The technique uses the local electrooptic coefficient to modulate the test optical pulse. More precisely, a local electric field induces a birefringence in the test electrooptic circuit substrate. The rotation of the plane of polarization is proportional to circuit voltage when the electrooptic coefficient is constant. The technique has been used successfully for testing numerous digital IC's and analog MMIC's [18-23].

In this work we use optical sampling to assess the electrical characteristics of the crystal material located directly below Ohmic contacts. In particular, the electrooptic sampling technique is used to noninvasively determine the electrical behavior of Ohmic contact regions in GaAs. The standard technique [24] for forming an Ohmic contact on a n^+ doped region in GaAs uses a mixture of AuGe/Ni/Au for the electrode formation. The Ohmic process possesses a complicated morphology. This diffusion mechanism may cause unexpected behavior in its crystal properties. For instance, diffusion of a Au/Ge/Ni/ mixture behaves differently than the individual diffusion of the metals if they are introduced separately [25]. Further complication arises because the local crystal defects that have grown through the epilayers generate non uniform migration of clusters of atoms during the Ohmic formation step [12].

Since the electrooptic sampling signal is proportional to the integrated electric field between the front and back surfaces of an electrooptic crystal (when a field is applied) weighed by an electrooptic coefficient such as r_{41} in GaAs, any deviation in the electrooptic coefficient from its nominal value will affect the results of the electrooptic sampling measurements. If the defect density introduced into a crystal during contact formation becomes high enough then a disruption in the crystal may be severe enough to affect the electrooptic coefficient. Thus, if the electrooptic coefficient is influenced by a cascade of defects introduced into the substrate then the electrooptic coefficient can be modeled as an activation energy dependent profile based on this diffusion. This will allow a spatially varying electrooptic coefficient to

modulate the detected optical signal revealing regions where high density defects exists.

This paper is organized as follows. Section II will discuss the CPW device tested as well as elucidate some of its electrical properties. Section III will discuss the electrooptical sampling arrangement as well as address some the calibration issues and accuracy of the technique. Section IV will then discuss some of the results obtained using the electrooptic sampling apparatus and present a simple phenomenological model based on a diffusion mechanism to explain the measured results. Finally, the conclusion section will review these results.

II. OHMIC COPLANAR WAVEGUIDE TEST DEVICE

The device tested is shown in fig. 1 and is a coplanar waveguide (CPW) device with an Ohmic Contact introduced by metalization placed over a heavily doped n^+ region in the substrate. Initially, the device consisted of a LEC grown wafer with two n^+ epilayers grown on top. The first layer is a 2800 Å epi-layer with a doping density of $2.1 \bullet 10^{17}$ cm^{-3} and the second a 940 Å n^{++} top epi-layer with a doping density of $3.9 \bullet 10^{18}$ cm^{-3}. Silicon (Si) was used as the dopant. Photoresist was applied in conjunction with a mask to pattern a region to be etched. Wet etching was used to remove the n^+ layers using a H_2SO_4(98%) /H_2O_2(30%) /H_2O solution in the ratio of 1:8:1000, to leave only 100μm wide strips of n^+ layers. The length of these strips varied from 300 to 2000 μm. A new mask was then used to deposit the AuGe(88%Au, 12%Ge)/Ni/Au layer which was then brought to 420° for 90 sec completing the Ohmic CPW. This is obviously a very large Ohmic but is ideally suited for

studying the effects of diffusion and how this diffusion affects the electrooptic coefficient. The final test device also consists of calibration test strips to calibrate on wafer s-parameter measurements. It will now be verified that the test device functions as a lossy transmission line.

Generally, a transmission line can be represented by a lumped element equivalent circuit as shown in fig. 2. The parameters defining this line are its resistance (R(ω)), inductance (L(ω)), capacitance (C(ω)), and conductance (G(ω)) per unit length. The parameters R(ω), L(ω), G(ω), and C(ω) are in general frequency dependent. With this model for an equivalent circuit in mind two important characteristics of a transmission line are its characteristic impedance Zo and its propagation constant. These can be expressed as follows:

$$Z_O=\sqrt{\frac{R(\omega)+j\omega L(\omega)}{G(\omega)+j\omega C(\omega)}} \qquad (1)$$

$$\gamma=\sqrt{(R(\omega)+j\omega L(\omega))\,(G(\omega)+j\omega C(\omega))} \qquad (2)$$

In these quasi TEM lines R(ω) and G(ω) usually represent loss where R(ω) is due to the finite conductivity of the metal and G(ω) is due to dielectric loss. The inductance (L(ω)) and the capacitance (C(ω)) are obviously the stored magnetic and electrical energy of the circuit and are not generally especially dependent upon frequency but are dependent upon the line geometry [26]

An HP8510 network analyzer was used in conjunction with a calibration program DEEMBED developed by Marks and William at NIST (to do on wafer calibration) to measure the electrical properties of the device [27-29]. These measured results are compared with a computer program developed by Heinrich [26],[30], which takes into account metalization conductivity,

thickness, and the dielectric substrate loss for CPW's. In other words the program takes into account the frequency dependence of R, G, and L; C is dependent only upon the geometry. The non-Ohmic test strips are very lossy due to the thin metalization (only about 1000 Å since liftoff was used to remove metalization on the devices). Figures 3a and 3b show the comparison of this program with the measured calibration strips for the propagation constants and impedance of lines which used the same metalization as that found over the n^+ strips. The conductivity used in the calculation was $1.5 * 10^7$ rather than the bulk value of $4 * 10^7$. It is expected that the conductivity would be lower for the evaporated metal. Excellent agreement is observed. S-parameter measurements confirm that the devices behave as very lossy lines. This was expected from the initial design of the CPW's since the n^+ regions have significantly lower conductivity than the metal lines ($\sigma \approx q\mu_n n$ where σ is the conductivity, q is the electronic charge, n is the doping density and, μ_n is the mobility assuming all the dopant is ionized and neglecting the hole contribution. $\sigma = 1/(R_s t)$ can also give the conductivity where R_s is the measured sheet resistance and t is the thickness of the doped layer). Figure 4 shows some typical s-parameter measurements of an Ohmic transmission line compared to the design done by Hewlett Packard's microwave design software (MDS). This particular CPW had a 700μm n^+ strip. The slight discrepancy is due to the frequency dependence of the transmission line parameters (mostly $R(\omega)$).

Transmission line theory was used to confirm that the fields of the CPW are actually known a priori. In a CPW it is known that if TEM wave is launched along the center conductor of this device, then at any point transverse to the direction of travel along the conductor, the field is constant

along this transverse direction (as long as the sampled point is not close to the edge [13]). Therefore we are presented with a slightly different problem in here than the usual problem of determining an unknown field distribution. Here the fields are known. The detected signal, however, is seen to vary with transverse dimension under some of the contacts which were sampled. Thus we are presented with the task of explaining this behavior. The importance of surface roughness and etalon effects important to the calibration of the electrooptic sampling technique will be addressed in the next section.

III. ELECTROOPTIC SAMPLING

The principle of operation of the electrooptic sampling is to use a non-zero electrooptic coefficient of a noncentrosymmetric substrate (GaAs in our case) to polarization modulate a probe beam and then to analyze that probe beam such that the detected signal is proportional to the circuit voltage [13-16]. The detected signal is then determined by the integrated electric field along a path normal to the surface as shown in fig. 5. If the electrooptic coefficient is not uniform throughout the crystal, then the detected voltage can be expressed as

$$I_{det} \approx V \approx \int r_{41}(x,y,z)\, E_y(x,y,z) \cdot dl \qquad (3)$$

where E_y is the normal directed field, dl is the normal path, and r_{41} is the electrooptic coefficient.

Although the lines are quite lossy due to the finite conductivity of the metals, the fields underneath the electrode at any transverse location of the

CPW can still be approximated by using the conformal mapping found in Symthe [31] and introduced by Wen [32] for finding the fields of CPW device. The mapping of the CPW into the interior of a rectangle is shown in fig. 6 and the solutions are shown below

$$E_x = -\frac{V}{K'(k)} \mathrm{Im}\left(\frac{dw}{dz}\right) \tag{5}$$

$$E_y = -\frac{V}{K'(k)} \mathrm{Re}\left(\frac{dw}{dz}\right) \tag{6}$$

$$\frac{dw}{dz} = \frac{1}{K'(k)} \frac{1}{\sqrt{(1-z^2)(1-z^2k^2)}} \tag{7}$$

The solution of the mapping is given by the Jacobi elliptic integral z= Sn(w,k) where k is the modulus. K(k) is the complete elliptical integral of the first kind. Now with this solution it would be merely an academic exercise to integrate the electric field along the normal path dl if it were not for the addition of the now spatially varying electrooptic coefficient which needs to go inside the integral.

The electrooptic sampling arrangement is shown in fig. 7. The detection of the optical signal uses time domain techniques analogous to a sampling oscilloscope to heterodyne the electromagnetic signal and the laser pulse. In this case a mode-locked laser pulse with a repetition rate of 76MHz and pulse width of 100ps is used as the probe beam. It interacts in the substrate with a high frequency electrical field having a frequency a multiple of the laser repetition rate plus an offset (of a 100KHz) to produce a ac signal of 100KHz which is an exact multiple of the high frequency electrical signal. The phase of the electrical signal can be recovered by either using a second synthesizer locked to the electrical signal which can be mixed down to the frequency of the detected optical signal to serve as a reference signal fed into

lock-in amplifier, or, by deriving the reference wave from the laser pulse itself as shown in the set-up. It is important to note that this system must maintain synchronism between the electrical signal and the laser sampling pulse. The wave plates serve to properly bias the probe beam so that maximum linear sensitivity is achieved. It should also be noted that the electrooptic sampling system provides two dimensional scans of the test device with position resolution of 1μm. The spot size of the optical sampling probe beam is 10μm.

Although electrooptic sampling provides great sensitivity (22 dB in GaAs) and is well suited to measuring the modulation of the test optical probe beam due to the local electrooptic coefficient, the detected signal requires careful processing. To accomplish this task, we have developed a calibration procedure for de-embedding the measured data which takes into account weak scattering and etalon effects of the substrate [13]. The success of this calibration procedure has been well documented for the fields of microstrip lines [13]. These calibration issues will be addressed. In particular the following issues will be addressed: 1) the thickness variations in the substrate, 2) the possibility of a spatially varying reflection coefficient, 3) the significance of a high backside reflection coefficient, and 4) scattering effects due to surface roughness.

Our analysis is based on long optical pulses compared to the substrate transit time since our wafer is approximately 600μm thick and the sampling pulses are approximately 100ps long. As previously stated [13] the optical probe beam enters an etalon formed by the CPW circuit giving a total reflection coefficient of

$$r(\phi_o) = \frac{-r_f + r_b e^{-i\phi_o}}{1 - r_f r_b e^{-i\phi_o}} \qquad (8)$$

where r_f and r_b are the effective reflection coefficients of the front and back surfaces of the GaAs substrate, and ϕ_o is the round trip phase delay of the etalon. Writing $r(\phi_o)$ as

$$r(\phi_o) = |r(\phi_o)| e^{-i\Phi(\phi_o)} \qquad (9)$$

and using the notation as stated earlier [13], the signal in the receiver head can be generally expressed as

$$\langle I_o \rangle = |r(\phi_o)|^2 \left[I^o_{dc} + \partial_{\phi_o} \Phi(\phi_o) I^o_{if} \right] \qquad (10)$$

I^o_{dc} and I^o_{if} represent the DC and IF receiver signal in the ideal case ($r(\phi_o) = 1$; $\partial_{\phi_o}\Phi = 1$) and do not depend on the substrate parameters, but only on the applied electrical field and the wave plate and crystal axes orientation in the sampling head. The detected signal is affected by an overall factor of $|r(\phi_o)|^2$ and the factor $\partial_{\phi_o}\Phi(\phi_o)$. The factor $|r(\phi_o)|^2$ is the DC receiver signal which is measured during the sampling scans and depends on the average total effective reflectivity of the substrate. The factor $\partial_{\phi_o}\Phi(\phi_o)$ is the wanted polarization rotation modulation giving rise to the AC signal but is also dependent upon the substrate parameters. The above factors will generally be spatially dependent. We have ignored the small scattering parameter which can reduce the effective contrast of the etalon and this will be justified shortly.

Since the metalization affects the optical properties of the substrate, knowledge of the CPW's fabrication will enable us to approximate the backside reflection coefficient. The front side reflection coefficient is approximated as a smooth optical interface between air and GaAs and is given by $(n_{GaAs}-1)/(n_{GaAs}+1) \approx .565$ since $n_{GaAs} \approx 3.6$. The metalization of the backside consist of a 520 Å layer of Au/Ge followed by a 100 Å layer of Ni and finally a 1000 Å layer of Au. The index of refraction of these metals are complex and are given as ($n=n_r + i \bullet n_i$ where $i=\sqrt{-1}$) $n_{Au} = .272 + i7.07$, $n_{Ge} = 4.42 + i(.123)$, and $n_{Ni} = 2.85 + i5.10$ (for $\lambda = 1.06\mu m$) [33]. The Ge layer does not seem to affect the result to any significant degree. Using a multilayer dielectric stack with complex indices of refraction [34], the back side reflection coefficient of the GaAs metal boundary was determined to be $|r_b| \approx .95$. The phase is just absorbed into the overall reflection coefficient. The importance of this high backside reflection coefficient is shown in figure 8 for $r_b = .95$ and $r_b = .9$. The Ac calibration factor $\partial_{\phi_0}\Phi(\phi_0)$ is shown as a function of phase retardation and does not have a very dramatic effect. Therefore the DC measured power may prove sufficient to calibrate the data. It should also be noticed that away from the resonance peak (away from where the relative phase is zero) the AC calibration is not significant. Therefore, if the scan was done on a relatively flat region (which DEKTAK measurements indicate in this case) then there would generally not be much calibration involved except for an absolute value factor. Although one would expect scattering from the Ohmic surface, it is primarily Rayleigh scattering and such high angle scattering is not detected by the detector anyway. To justify our calibration we refer to fig. 9. The sample is scanned twice along the center conductor with the sampling points placed in increments of 30 μm apart. Figure 9c shows the scanning region. Figure 9(a) shows the electrooptic signal and 9(b) shows the average optical detected

power. It should be noted that the roughness in surface is present in the non Ohmic overlapping metal regions also. The pure n^+ regions are obviously smooth. Trial 2 is the same as scan 1 except that the probe beam is moved 10 μm transversely to the scan in trial 1. The two scans should be identical. Normalizing the detected electrooptic signal to the average optical power appears to calibrate the data quite effectively. This is shown in fig 10. This fact is further evidenced in noting that the raw data variations precisely mimic the average power variations. Also, if the average power is constant (indicating very little substrate thickness variation) then the AC calibration factor should not affected much either since this calibration factor is highly dependent upon these thickness variations. Finally, there could exist a spatially varying reflection coefficient that would complicate the data even more since there are not enough known factors to calibrate this effect However this effect would also show up in the DC power scan and therefore it is still possible to provide an accurate calibration. Figure 9 also demonstrates the repeatability of the data.

Electrooptic sampling results are sensitive to the electrooptic coefficient. Therefore, lattice disruption (disordering) severe enough to affect the electrooptic coefficient will be observed. Since diffusion occurs under Ohmic contacts has been demonstrated [12], a diffusion model seems appropriate to explain how lattice disruption can take place. Accurate diffusion modeling is complicated. Implanting Si as a dopant (Si was used as our dopant) already has caused impurity induced disordering (IID) [35]. The model to be discussed here will therefore be somewhat qualitative in nature.

In volumes where a significant amount of microprecipitate diffusion has taken place, it is safe to assume the lattice is disrupted. It might prove useful to compare the integrated electric field (between the front and back surfaces of the circuit substrate) weighed by a constant electrooptic coefficient to that of the integrated electric field (voltage) when the electrooptic coefficient is totally disrupted some known distance below the contact to estimate the order of the effect which would be measured. This is shown in fig. 11. The electric fields used are for a CPW device and the probing beam size is assumed to be a delta function like beam spatially. In this figure the amount of deviation from the ideal voltage signal (in dB) is plotted as a function of the depth from the electrode surface which has had its electrooptic coefficient totally nulled. For example, if in the first 10 μm below the device has a zero electrooptic coefficient, then the detected voltage signal would be down -3 dB from its ideal non affected electrooptic coefficient. With a disrupted electrooptic coefficient extending 20 μm into the substrate below the contact electrodes would result in a - 5.5 dB reduction in the detected signal. We can compare this resulting variation in signal with that of the measured data shown in fig. 12. Figure 12(a) and 12(b) show the raw data of an electrooptic scan of a CPW test device. Figure 12(c) shows the area scanned. It can be seen in this case that the average power along the n+ and Ohmic regions are very constant. This is generally true for very small scan regions. Therefore no real calibration is necessary here (except for an absolute value correction). Here the scanning sampling points are 10 μm apart longitudinally. A maximum variation of 8 dB is observed along the transverse location of the transmission line when present in the Ohmic region. Trials 1, 2 and 3 are all along the center conductor except spaced 5 μm apart in the transverse direction. Since the signal should remain constant at any identical transverse

location on the CPW this perturbation is due to the electrooptic coefficient and not the applied electric field. This 8 dB variation would correspond to the nulling of the electrooptic coefficient down to a depth of approximately 30 μm. This seems higher than one might expect but it is the extreme case measured (of 20 devices fabricated) and gross dislocations in the substrate could account for this behavior. Consideration of our diffusion model will now be addressed.

The electrooptic signal is given as in eq. (3). Ignoring the spatial extent of the probing beam (the overlap integral of the 10 μm beam will result in a slightly smaller detected perturbation in the signal but to avoid unnecessary complicated expressions will be ignored) the detected signal can again be written as

$$I_{det} \approx V \approx \int r_{41}(x,y,z)\, E_y(x,y,z) \cdot dl \qquad (11)$$

It was just demonstrated that a direct nulling of the electrooptic coefficient below the CPW electrode can alter the sampling signal significantly if this destruction occurs over several microns. If the electrooptic coefficient (r_{41}) is modified by a diffusion process then this diffusion could explain why our detected signal deviates from the expected. A simple one-dimensional model based on Fick's law of diffusion will be used [36]. Combining Fick's first and second laws gives the following equation and is used for the rate of concentration impurities diffusing into the GaAs substrate (y direction)

$$\partial N/\partial t = \partial/\partial y\, [\, D\, \partial N/\partial y\,] \qquad (12)$$

where in general the diffusion coefficient is dependent upon depth if it involves high impurity concentrations [36]. Here N=N(y,t) is the concentration of impurities and D is the diffusion coefficient. However it was observed in Baeumler's work [4] that defects can propagate through the epilayers to the surface. This will make the a spatial variation in the diffusion coefficient as a function of depth constant but will give the diffusion coefficient a spatial variation (depending where there are defects dictates its magnitude). Therefore eq. (12) becomes

$$\partial N/\partial t = D(x,z)\ \partial^2 N/\partial^2 y \qquad (13)$$

where D(x,z) possess spatial variation. If we solve this equation assuming a constant diffusion source the following solution is obtained

$$N(y,t) = N_o\ \mathrm{Erfc}[y/(2\sqrt{Dt})] \qquad (14)$$

Here, N_o is the impurity and Erfc is the complementary error function. Since our model is purely phenomenological, the meaning of N_o , N(y,t), and the diffusion coefficient should be discussed. The diffusion coefficient will assume to follow an Arrhenius behavior and is given by

$$D = D_o \exp[-E_A/(kT)] \qquad (15)$$

where D_o is the diffusion constant, k is the Boltzman constant, T is the temperature at which the diffusion takes place, and E_A is the activation energy. High temperatures normally involved in diffusion models mitigate the sensitivity of the activation energy. However, in our model the activation

energy is viewed as simply a defect activated energy dependent upon the defect concentration and is highly sensitive to small variations in this activation energy. Additionally, since the diffusion constant is unknown these values need to be determined. Figure 13 shows the variation of the diffusion $N(y,t)/N_o$ as function of depth in μm for various diffusion constants and activation energies. There is dramatic effect on $N(y,t)/N_o$ for different activation energies. This corresponds to the defects presence to rapidly increase diffusion below the electrode. However, the effect $N(y,t)/N_o$ has on the disruption of the electrooptic coefficient needs clarification. If we assume that as long as $N(y,t)/N_o$ exceeds some nominal value of 1% results in a volume with a greatly reduced electrooptic coefficient, then figure 14 shows that an activation energy of 1.3eV and diffusion constant of 10 cm^2/s dictates that this volume extends to a depth of approximately 20μm. Using this hard limit of

$$r_{41}=\begin{cases} r_{41}, & N(y,t)/N_o < .01 \\ 0 & N(y,t)/N_o > .01 \end{cases} \qquad (16)$$

results in agreement with our measured data. The meaning of $N(y,t)/N_o$ however remains nebulous. The assumption of the 1% rule generally referred to interstitial type of defects. Therefore the question remains if these precipitate defects are for example, approximately nanometer in size with a density of 10^{16} to 10^{18} cm^{-3} [12], then how does the quantify the meaning of $N(y,t)/N_o$. For example, does a nanometer size particle which is approximately 1000 lattice sites in size dictate that it will affect the electrooptic coefficient for 100,000 lattice sites? The answer to this question does not necessarily need to

be answered since the real answer to our problem presented here is that electrooptical sampling can detect a reduction of the electrooptic coefficient.

V. CONCLUSION

We have presented the results of electrooptical sampling on unique Ohmic contact coplanar waveguides (CPW's). A reduced electrooptical sampling signal was detected in certain Ohmic contact regions. This reduced signal is attributed to a nulling of the electrooptical coefficient. A mechanism contributing to the reduced electrooptical coefficient is presented and is based on a phenomenological model incorporating diffusion processes. This model takes into account defects introduced into the substrate during the annealing step of Ohmic contact fabrication that may be severe enough to disrupt the crystal properties that would result in a reduced electrooptical coefficient. This simple diffusion model uses a spatially varying activation energy based on the defect density and agrees with our results. Calibration issues concerning the electrooptical sampling technique are addressed and do not appear to effect the measured data significantly.

It should be noted that we have used electrooptical sampling in a different manner than the usual procedure of determining unknown field distributions. Here, the fields are known but the electrooptic coefficient is seen to vary spatially below the Ohmic surface. This new application of electrooptical sampling could be used, for example, to possibly measure the electrooptic coefficient perturbation present in $LiNbO_3$ waveguides when proton exchange (H+ ions) occurs or Ti in diffusion takes place. Furthermore, a low frequency version of optical sampling technique could be used for more

expedient and less sophisticated instrumentation to measure semiconductor characteristics.

ACKNOWLEDGMENT

The authors are grateful for the valuable discussions with J. P. Fillard, M. Castagné, P. C. Montgomery of the Laboratoire LINCS-CEM Université de Montpellier, and with M. Baeumler and W. Jantz of the Fraunhofer Institut für Angewandte Festkörperphysik. This work was supported by the Army Research Office under Grant #DAAL-03-92-G-0289 and by the Office of Naval Research Grant #DOD-ONRN00014-92-J-1190.

REFERENCES

[1] C. Miner, "Pre-processing epitaxial layer evaluation: What do you really measure?," *Inst. Phys. Conf. Ser.* No. 135 Ch. 5 pp. 147-156, 1994.

[2] V. P. Kalinushkin, N. V. Safronov, N. A. Sulimov, "Spatial orientation study of microprecipitates in Semi-insulating GaAs crystals by IR light scattering technique," *Inst. Phys. Conf. Ser.* No. 135 Ch. 4 pp. 143-146, 1994.

[3] P. Franzosi, H. Bernardi, "Investigation of extended crystal defects in HgCdTe epilayers on CdTe, CdZnTe and CdTe/sapphire,"*Inst. Phys. Conf. Ser.* No. 135 Ch. 9 pp. 319-322, 1994.

[4] M. Baeumler, E. C. Larkins, K. H. Bachem, D. Bernklan, H. Riechert, J. D. Ralston, W Jantz, "Influence of substrate dislocations on epitaxial layers studied by

photoluminescence microscopy and topography,"*Inst. Phys. Conf. Ser.* No. 135 Ch. 5 pp. 169-172, 1994.

[5] P. Gall, J. P. Fillard, M. Castagné, J. L. Weyher, J. Bonnafé, "Microtomagraphy observation of precipitates in semi-insulating GaAs materials," *J. Appl. Phys.* **64**, (10) 15, Nov., 1988.

[6] J. P. Fillard, P. C. Montgomery, P. Gall, M. Castagné, J. Bonnafé, "High Resolution and Sensitivity Infrared Tomography," *J. Crystal Growth* , **103**, pp. 109-115, 1990.

[7] J. P. Fillard, M. Castagné, P. Gall, J. Bonnafé, "Tranistor specifications and substrate defects in GaAs test circuits," J GaAs Application Symposium (Rome), 1990.

[8] M. Castagné, J. P. Fillard, D. Achvar, P. Gall, "LST-detected microprecipitates and their role in the performance of GaAs integrated circuits," *Semicon. Sci. Technol.*, **7**, A146-A149, 1992.

[9] S. Miyazawa, Y. Ishii, S. Ishida, Y. Nanishi, "Direct observation of dislocation effects on threshold voltage of a GaAs field-effect transistor," *Appl. Phys. Lett.* **43** (9), 1, Nov. 1983.

[10] F. Hyuga, "Effect of dislocations on sheet carrier concentration of Si-Implanted, Semi-Insulating, Liquid-Encapsulated Czochralski grown GaAs,"

[11] Z. M. Wang, M. Baeumler, W. Jantz, K. H. Bachem, E. C. Larkins, J. D. Ralston, "Photoluminescence microscopy investigation of lattice defects in epitaxial heterostructures," *J. Crystal Growth*, **126**, pp. 205-215, 1993.

[12] J. P. Fillard, M. Castagné, P. C. Montgomery, J. Bonnafé, P. Gall, E. Baudry, D Montaner, "Latest results in interface image reconstruction: Application to ohmic contact inspection," *Inst. Phys. Conf. Ser.* No. 135 Ch. 4 pp. 109-116, 1994.

[13] D. R. Hjelme, A. R. Mickelson, "Voltage Calibration of the Direct Electrooptic Sampling Technique," IEEE *J.Trans. Microwave Theory Tech.*, **40**, no. 10, pp. 10 1941-1950, 1992.

[14] J. A. Valdmanis, G. Mourou, "Sub-picosecond electro-optic sampling: Principles and applications," IEEE *J. Quantum ELectron.*, **QE-22**, pp. 69-78, 1986.

[15] B. H. Kolner, D. M. Bloom, "Electrooptic sampling in GaAs integrated circuits,"IEEE *J. Quantum ELectron.*, **QE-22**, pp. 79-93, 1986.

[16] K. J. Weingarten, M. J. Rodwell, D. M. Bloom, "Picosecond optical sampling of GaAs integrated circuits," IEEE *J. Quantum ELectron.*, **QE-24**, pp. 189-220, 1988

[17] J. M. Wiesenfeld, "Electro-optic sampling of high-speed devices and integrated circuits," IBM *J. Res. Develop.*, **34**, pp. 141-161, 1990.

[18] R. Majidi-Ahy, K. J. Weingarten, M. Riaziat, B. A. Auld, D. M. Bloom, "Electrooptic sampling measurements of coplanar waveguide modes," *Electr. Lett.*, **23**, pp. 1262-1263, 1988.

[19] K. J. Weingarten M. J. Rodwell, D. M. Bloom, "Picosecond optical characterization of GaAs integrated circuits," *Gallium Arsenide Tech.*, Vols II-III, Ed. D.K. Ferry, 1987.

[20] J. L. Freeman, S. K. Diamond, H. Fong, D. M. Bloom, "Electro-optic sampling of planar digital GaAs integrated circuits", *Appl. Phys. Lett.*, **47**, pp. 1083-1084, 1985.

[21] M. J. Rodwell, K. J. Weingarten, J. L. Freeman, D. M. Bloom, "Gate propagation delay and logic timing of GaAs integrated circuits measured by electro-optic sampling," *Electron. Lett.*, **22**, pp. 499-501,1986.

[22] X. C. Zhang, R. K. Jain, "Measurement of on-chip waveforms and pulse propagation in digital integrated circuits by electro-optic sampling," *ELectron. Lett.*, **22**, pp. 264-265, 1986.

[23] J. M. Wiesenfeld, R. S. Tucker, A. Antreasyan, C. A. Burrus, A. J. Taylor, V. D. Mattera, P. A. Garbinski, "Electro-optic sampling measurements of high speed InP integrated circuits," *Appl. Phys. Lett.*, **50**, pp. 1310-1312, 1987.

[24] N. Braslau, " Ohmic Contacts to GaAs," *Thin Solid Films*, **104**, pp. 391-397, 1983.

[25] M. Heiblum, M. I. Nathan, C A. Chang, "Characteristics of AuGeNi Ohmic Contacts to GaAs," Solid State Electr. 25, no. 3 pp. 185-195, 1982,

[26] W. Heinrich, "Full-Wave Analysis of Conductor Losses on MMIC Transmission lines," IEEE *Trans. Microwave Theory Techniques*, **38**, no. 10., pp. 1468-1472, 1990.

[27] R. B. Marks, "A Multiline Method of Network Analyzer Calibration," IEEE *Trans. Microwave Theory Techniques*, **39**, no. 7., pp. 1205-1215, 1991.

[28] R. B. Marks, D. F. Williams, " Characteristic Impedance Determination Using Propagation Constant Measurement," *Microwave and Guided Wave Letters*, **1**, no. 6., pp. 141-143, 1991.

[29] D. F. Williams, R. B. Marks, "Transmission Line Capacitance Measurement," *Microwave and Guided Wave Letters*, **1**, no. 9., pp. 243-245, 1991.

[30] W. Heinrich, "Quasi-TEM Description of MMIC Coplanar Lines Including Conductor-Loss Effects," IEEE *Trans. Microwave Theory Techniques*, **41**, no. 1., pp. 45-52, 1993.

[31] W. R. Smythe, *Static and Dynamic Electricity*, Third ed. Hemisphere Publishing Corporation, New York, pp. 101-102.

[32] C. P. Wen, "Coplanar Waveguide: A Surface Strip Transmission Line Suitable for Non reciprocal Gyromagnetic Device Application," IEEE *Trans. Microwave Theory Techniques*, **17**, , pp. 1087-1090, 1969.

[33] Handbook of Optical Constants fo Solids I-II, Ed. by E. D. Palik, Academic Press, Inc.

[34] M. Born, E. Wolf, *Principles of Optics*, sixth ed., Pergamon Press, Oxford, 1980.

[35] B. Chen, Q. M. Zhang, J. Bernhok, "Si diffusion in GaAs and Si-induced interdiffusion in GaAs/AlAs superlattices," *Phy.s Rev. B*, **49**, no. 4, pp. 2985-2988, 1994.

[36] R. C. Jaeger, *Introduction to Microelectronic Fabrication*. Vol. 5, Modular Series on Solid State Devices, Ed. G. W. Neudeck, R. F. Pierret, Addison-Wesley Pub., Co. 1989.

FIGURE CAPTIONS

Fig. 1 Ohmic CPW test device.

Fig. 2 Transmission line equivalent circuit.

Fig. 3 Transmission Line parameters of calibration strips.

3a) Impedance of CPW line - measured vs. Heinrich.

3b) Propagation constants of CPW line - measured vs. Heinrich.

Fig 4 S-parameters of Ohmic CPW

Fig. 5 Optical sampling substrate geometry.

Fig. 6 CPW conformal mapping to determine electric fields.

Fig. 7 Optical sampling experimental arrangement.

Fig. 8 AC calibration factors present due to the circuit substrate.

Fig. 9 Measured electrooptical Data of Ohmic CPW line.

9(a) Raw E-O sampling detected voltage.

9(b) Average optical detected Power - used for calibration.

9(c) Scanning area under CPW line.

Fig. 10 Calibrated electrooptical sampling data.

Fig. 11 Deviation in electrooptic signal vs. depth of nulled electrooptical coefficient.

Fig. 12 Measured electrooptical data in the Ohmic region of a CPW line.

12(a) Raw E-O sampling data.

12(b) Average optical detected power.

12(c) Scanning area under CPW line.

Fig. 13 Effective defect concentration Vs depth below Ohmic surface.

13(a) Diffusion constant = 1 cm^2/s, EA=1.3, 1.5, 1.7 eV

13(b) Diffusion constant = 10 cm^2/s, EA=1.3, 1.5, 1.7 eV

13(c) Diffusion constant = 100 cm^2/s, EA=1.3, 1.5, 1.7 eV

Fig. 14 Effective defect concentration for Do = 10 cm^2/s, EA=1.3, 1.4 eV

Ohmic CPW

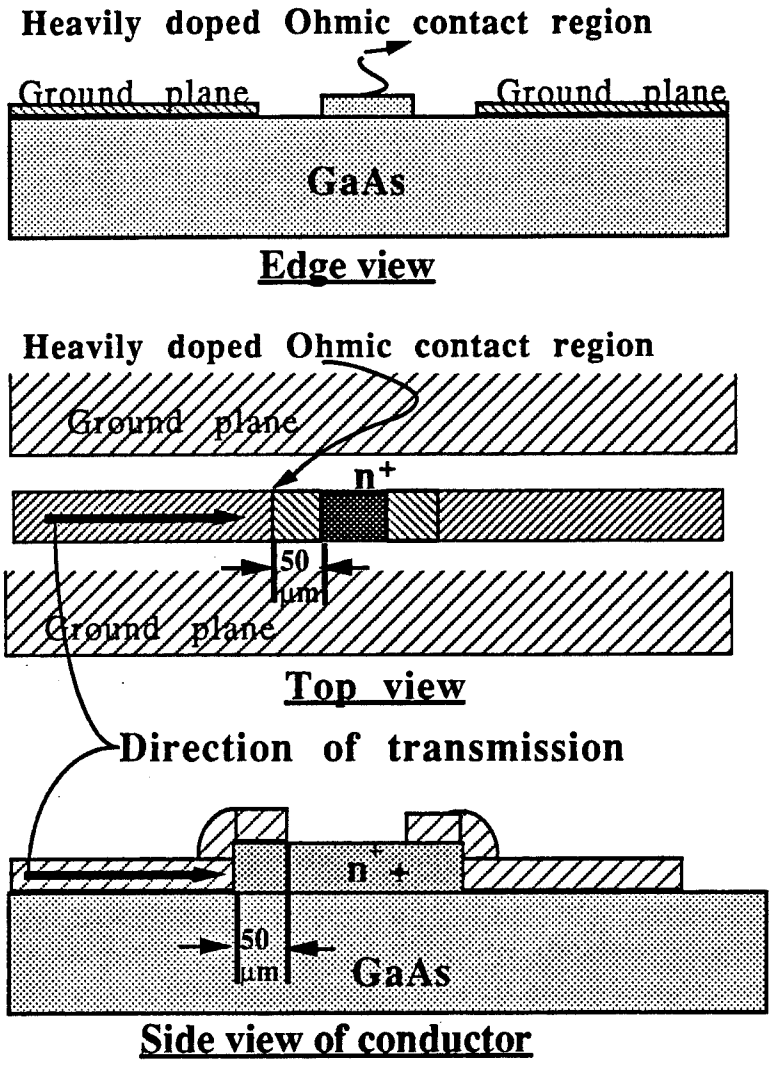

Fig 1

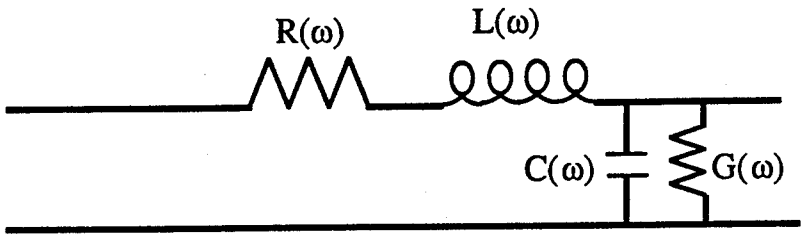

Fig 2

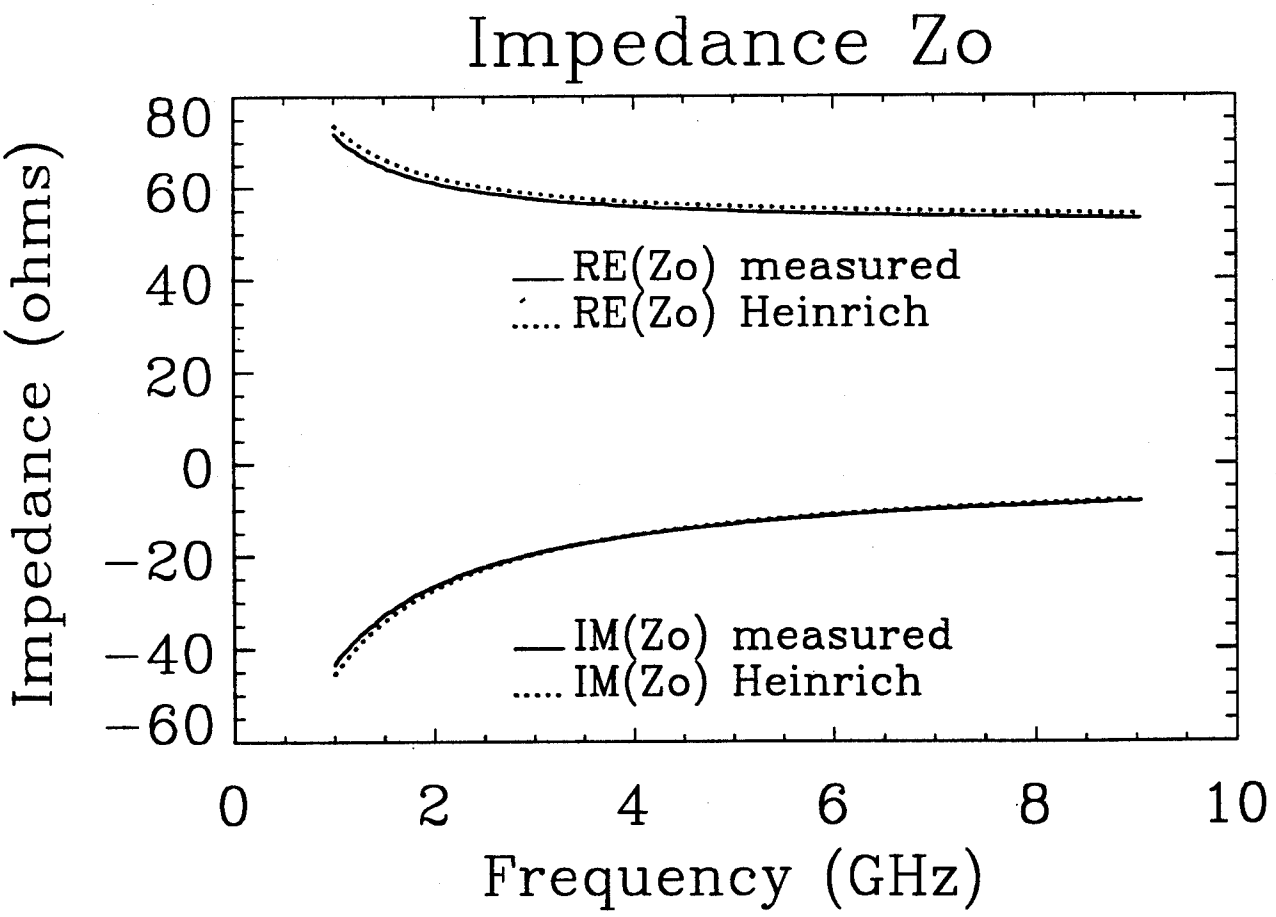
Impedance Zo
Impedance (ohms)
80
60
40
20
0
−20
−40
−60
RE(Zo) measured
RE(Zo) Heinrich
IM(Zo) measured
IM(Zo) Heinrich
0
2
4
6
8
10
Frequency (GHz)

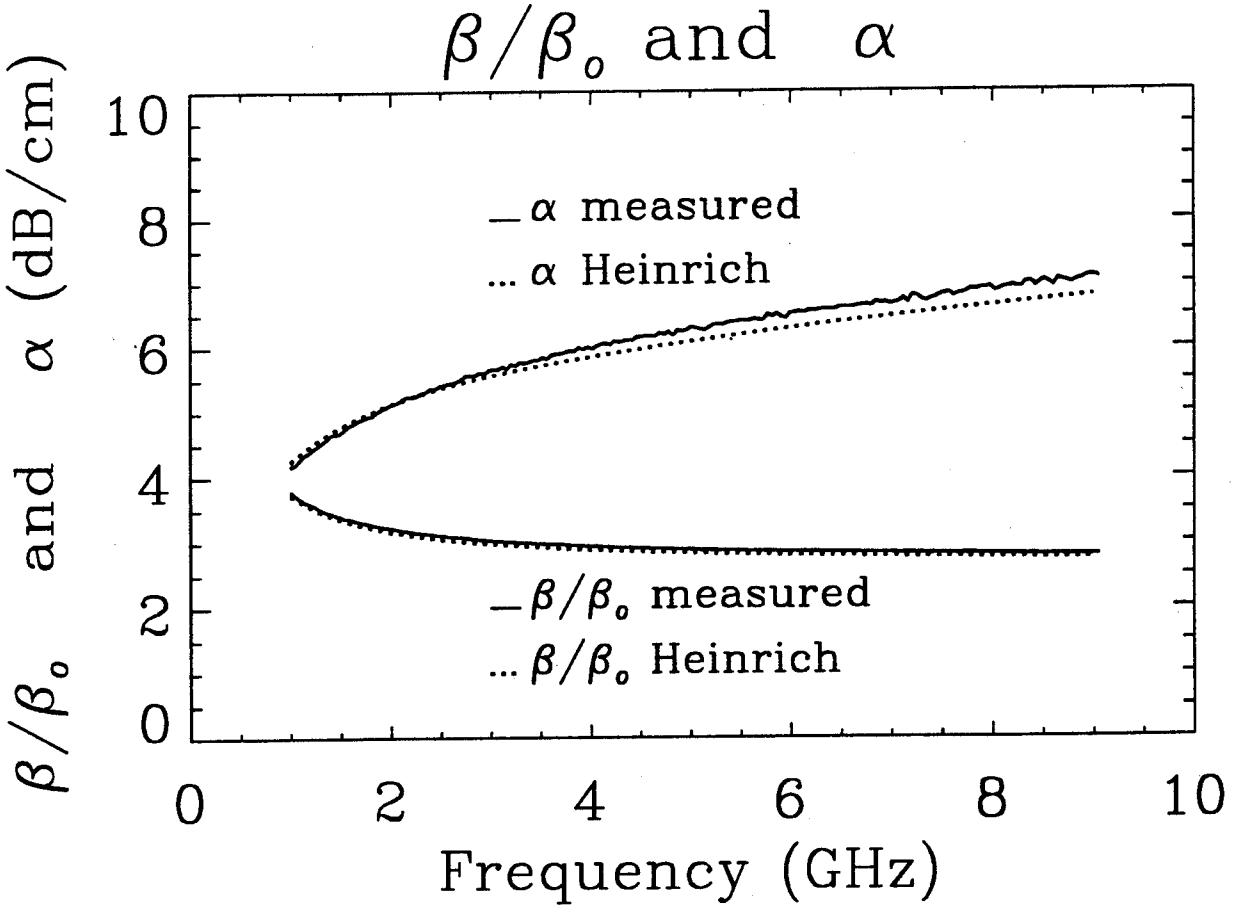
β/β₀ and α
β/β₀ and α (dB/cm)
10
8
6
4
2
0
0
2
4
6
8
10
Frequency (GHz)
α measured
α Heinrich
β/β₀ measured
β/β₀ Heinrich

3B

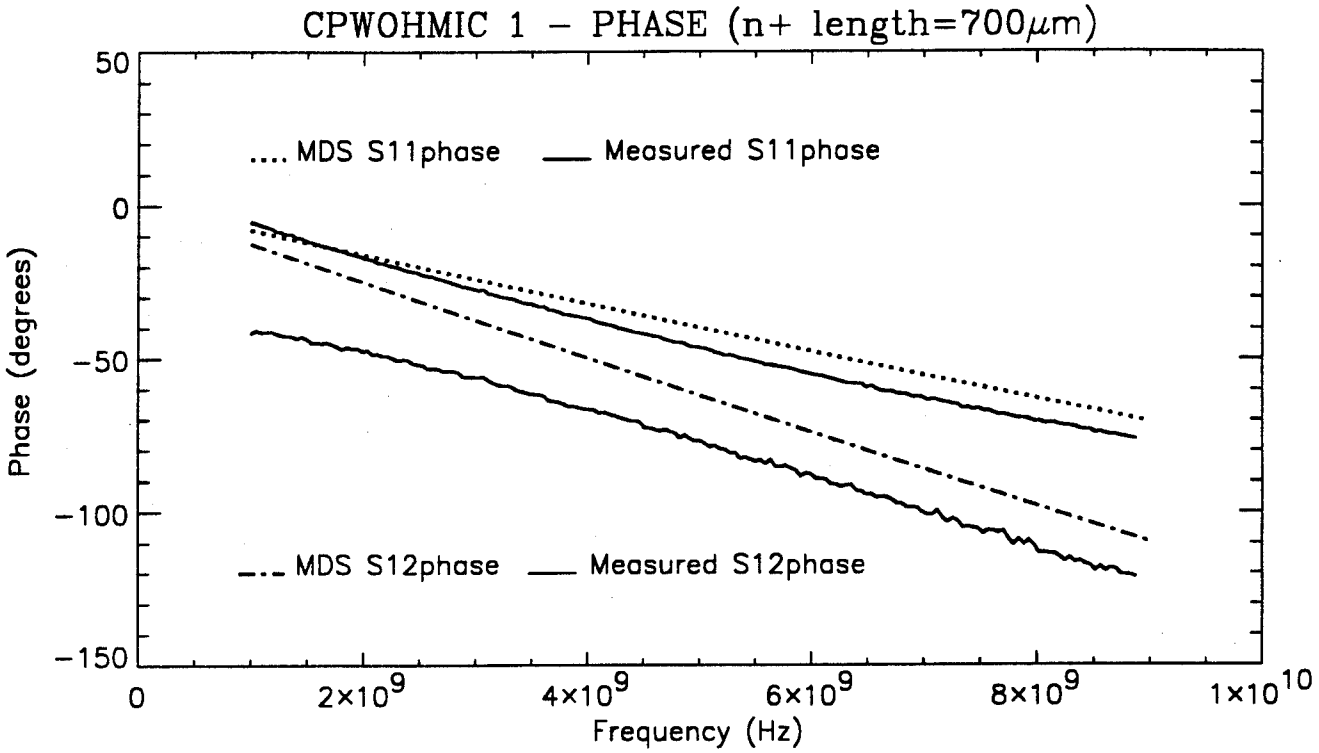
CPWOHMIC 1 – PHASE (n+ length=700μm)
50
0
−50
−100
−150
Phase (degrees)
.... MDS S11phase
Measured S11phase
MDS S12phase
Measured S12phase
0
2×10^9
4×10^9
6×10^9
8×10^9
1×10^10
Frequency (Hz)

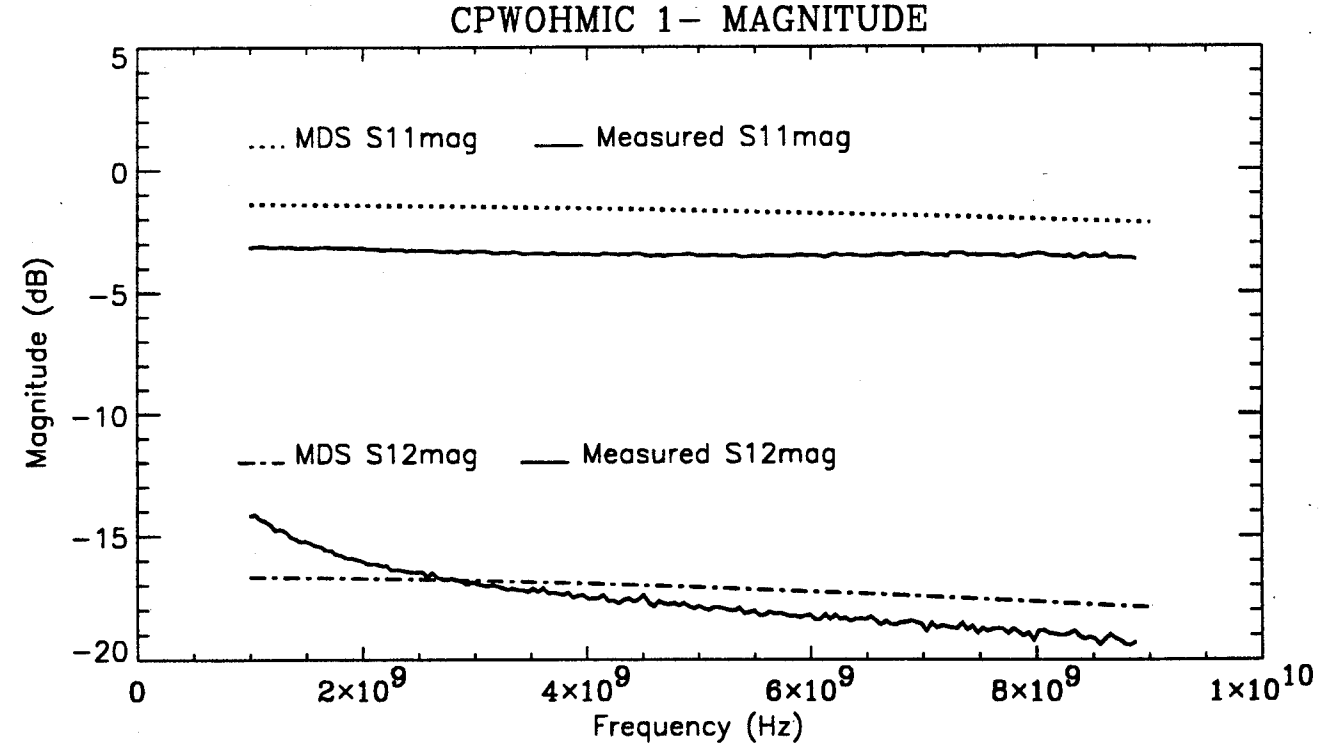
CPWOHMIC 1– MAGNITUDE
5
0
−5
−10
−15
−20
Magnitude (dB)
.... MDS S11mag
Measured S11mag
MDS S12mag
Measured S12mag
0
2×10^9
4×10^9
6×10^9
8×10^9
1×10^10
Frequency (Hz)

Fig 4

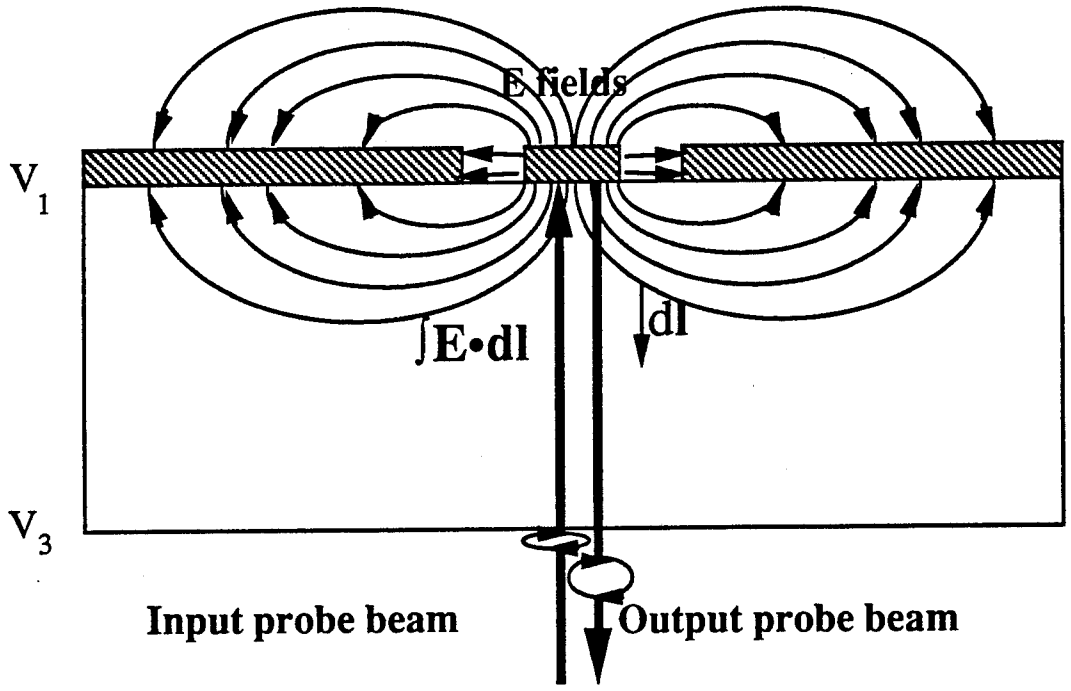

Fig 5

CPW Conformal Mapping

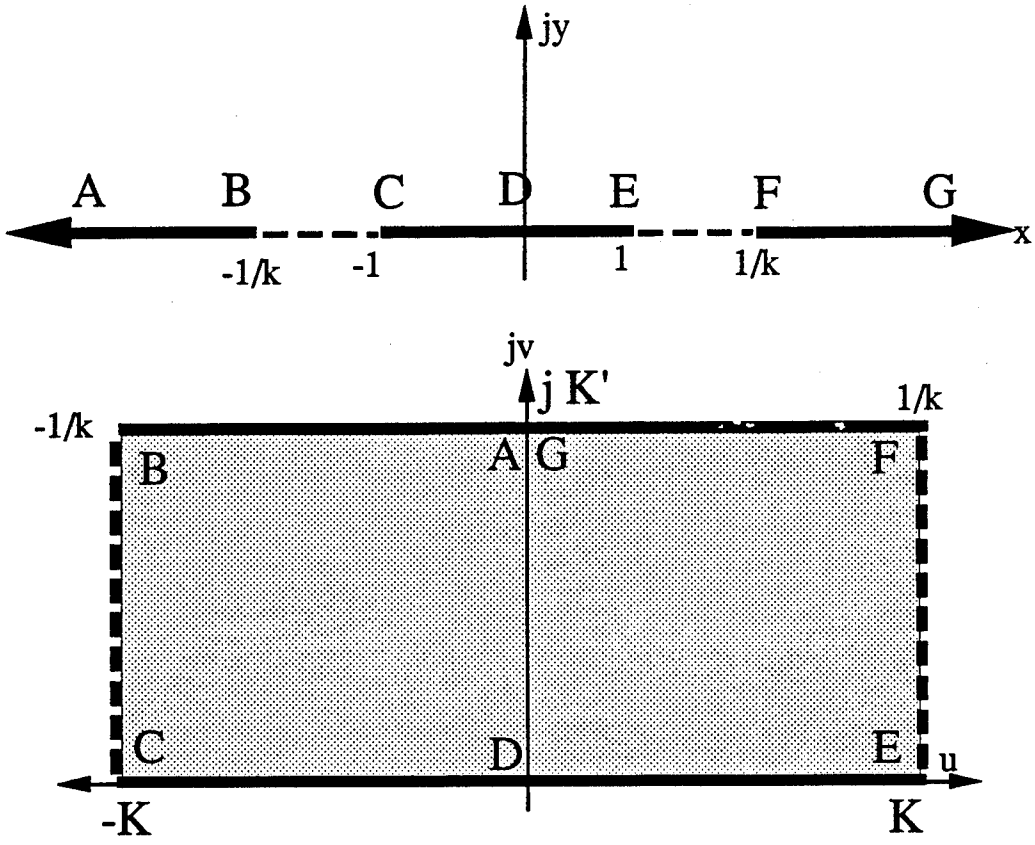

Fig 6

Phase and Amplitude Measurement

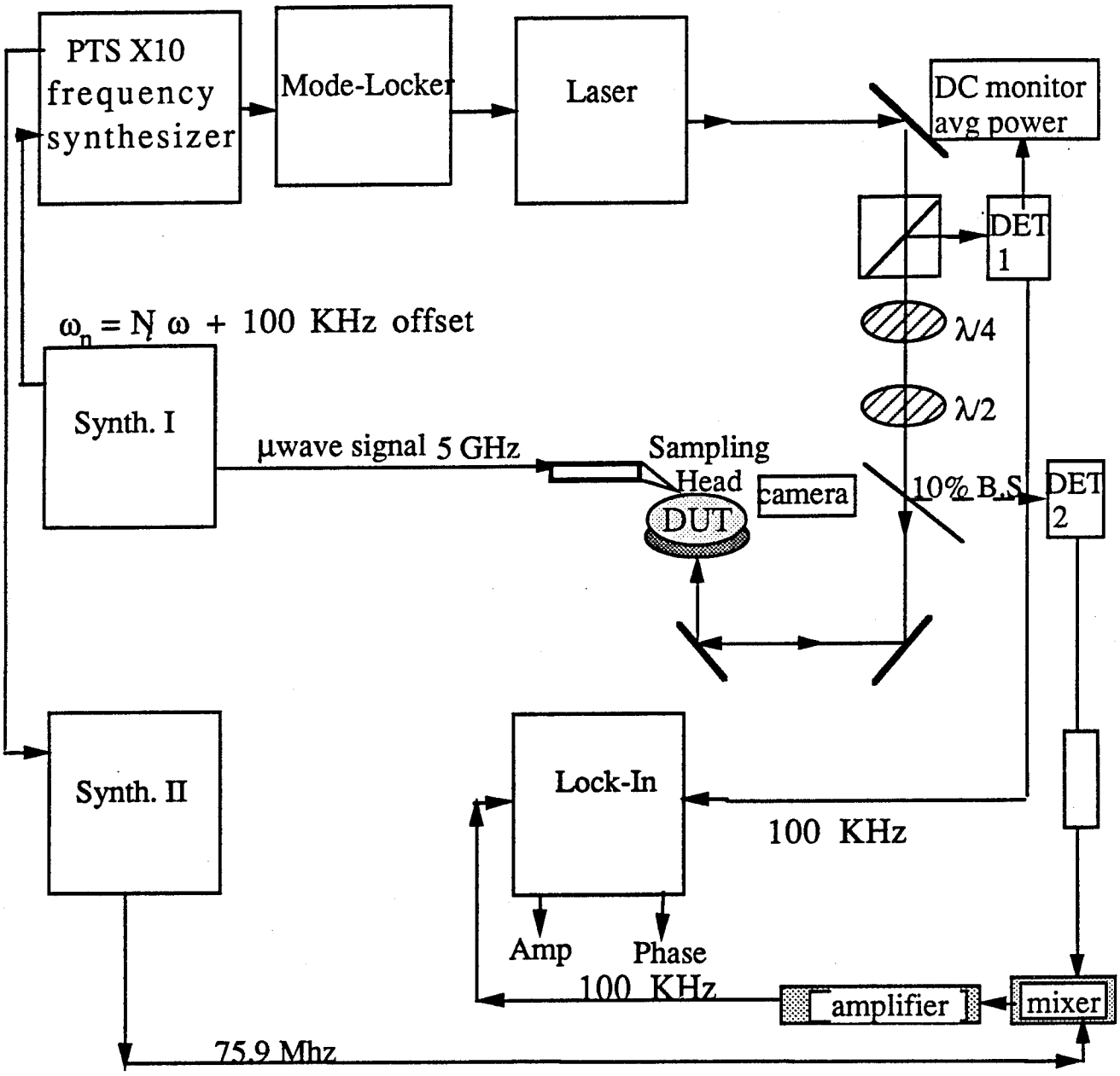

Fig 7

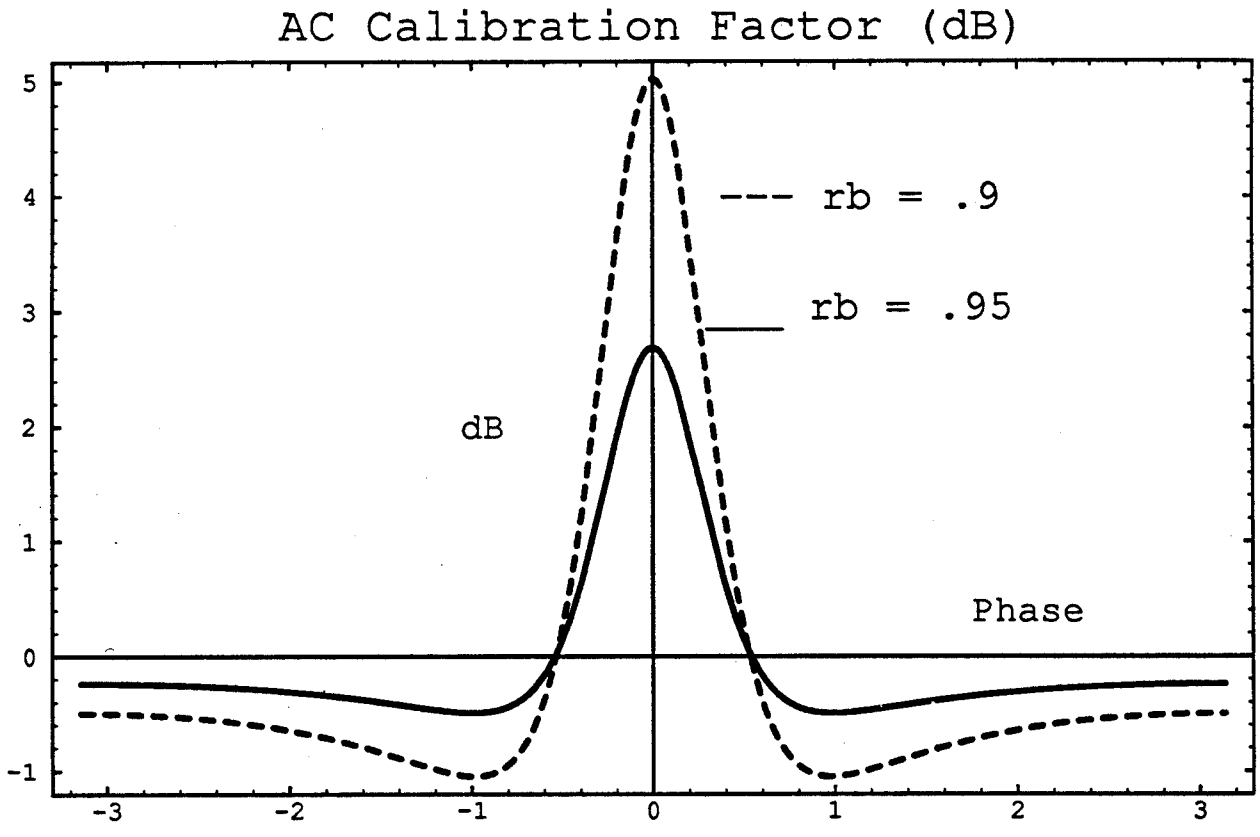

Fig 8

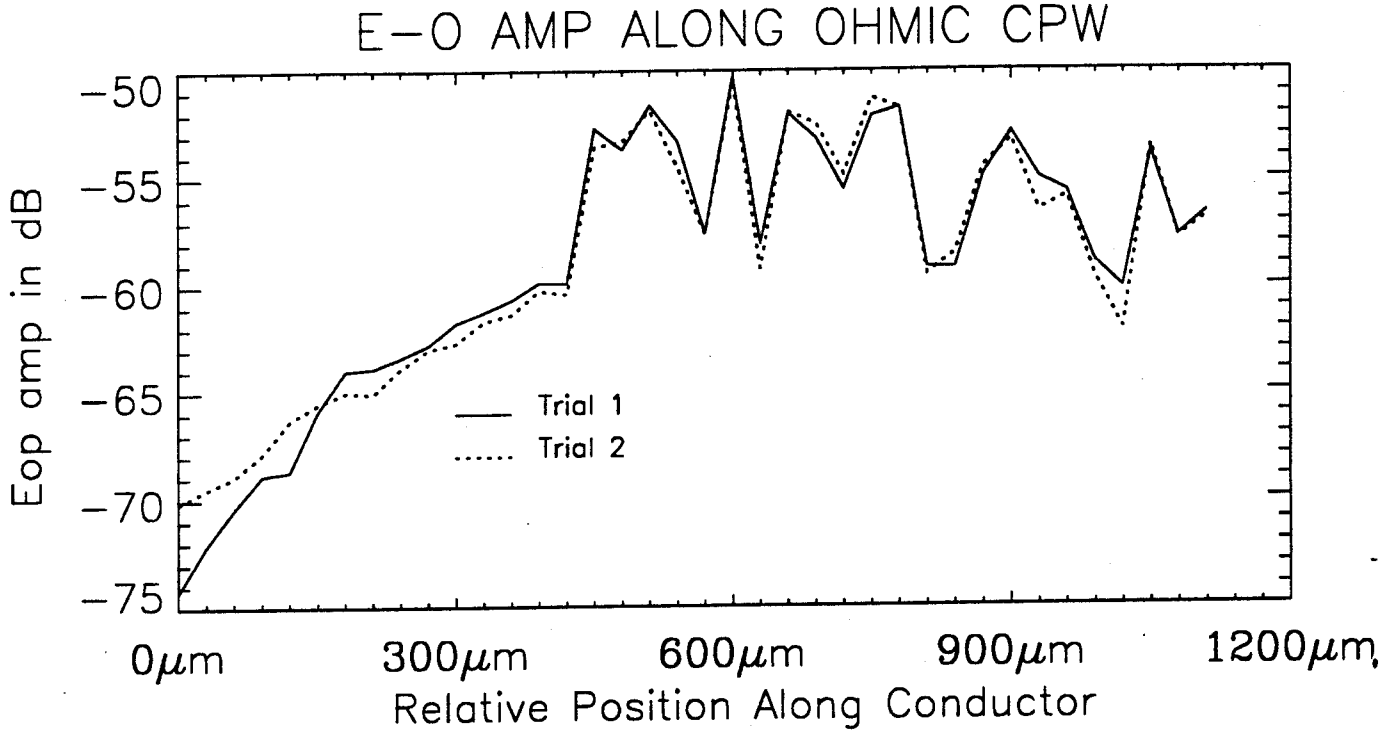
E–O AMP ALONG OHMIC CPW
Eop amp in dB
−50
−55
−60
−65
−70
−75
Trial 1
Trial 2
0μm
300μm
600μm
900μm
1200μm
Relative Position Along Conductor

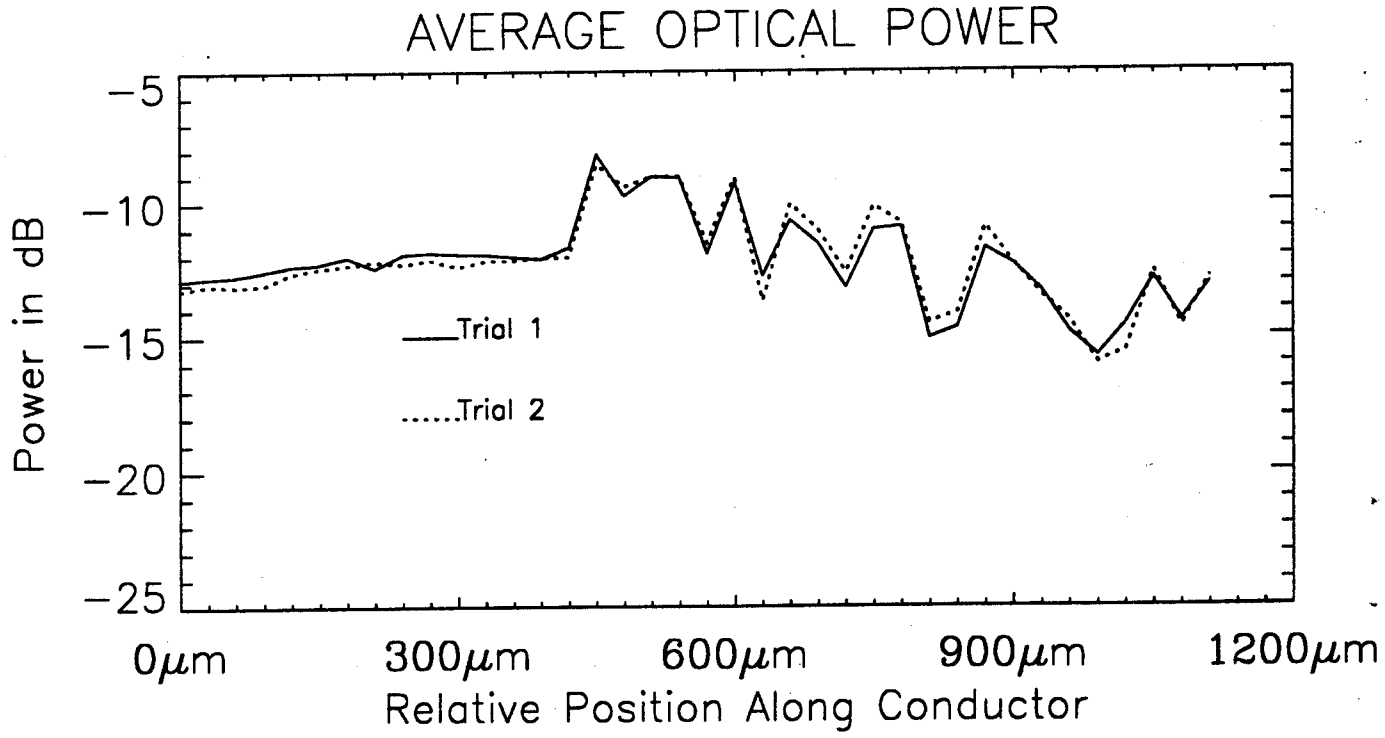
AVERAGE OPTICAL POWER
Power in dB
−5
−10
−15
−20
−25
Trial 1
Trial 2
0μm
300μm
600μm
900μm
1200μm
Relative Position Along Conductor

Γ. 1 a d (1)

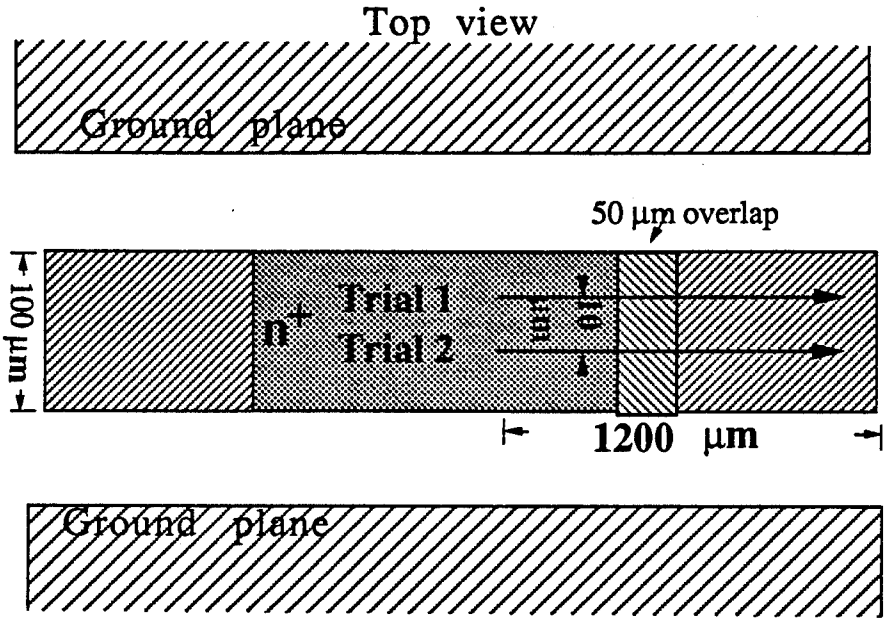
Top view
Ground plane
50 μm overlap
100 μm
n+
Trial 1
Trial 2
100 μm
1200 μm
Ground plane

Fig 9c

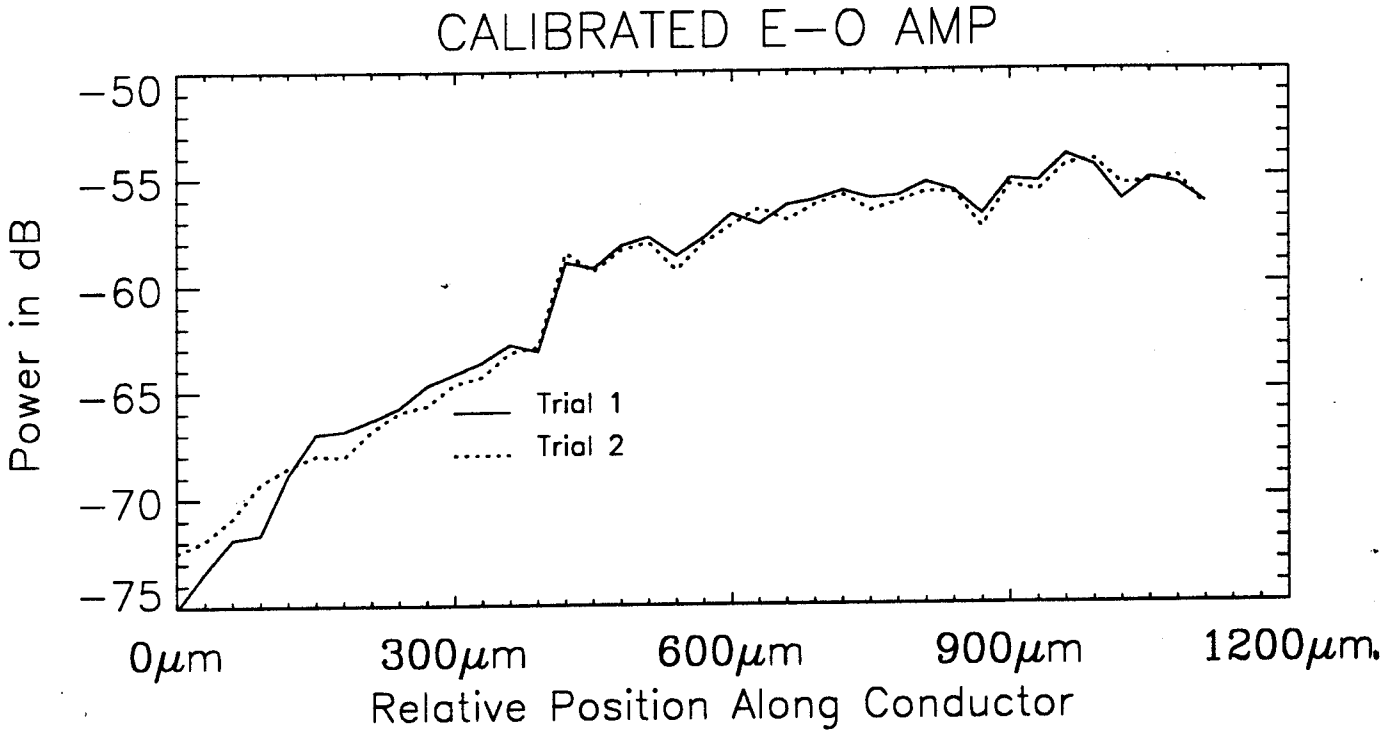
CALIBRATED E-O AMP
Power in dB
−50
−55
−60
−65
−70
−75
Trial 1
Trial 2
0μm
300μm
600μm
900μm
1200μm.
Relative Position Along Conductor

Fig 10

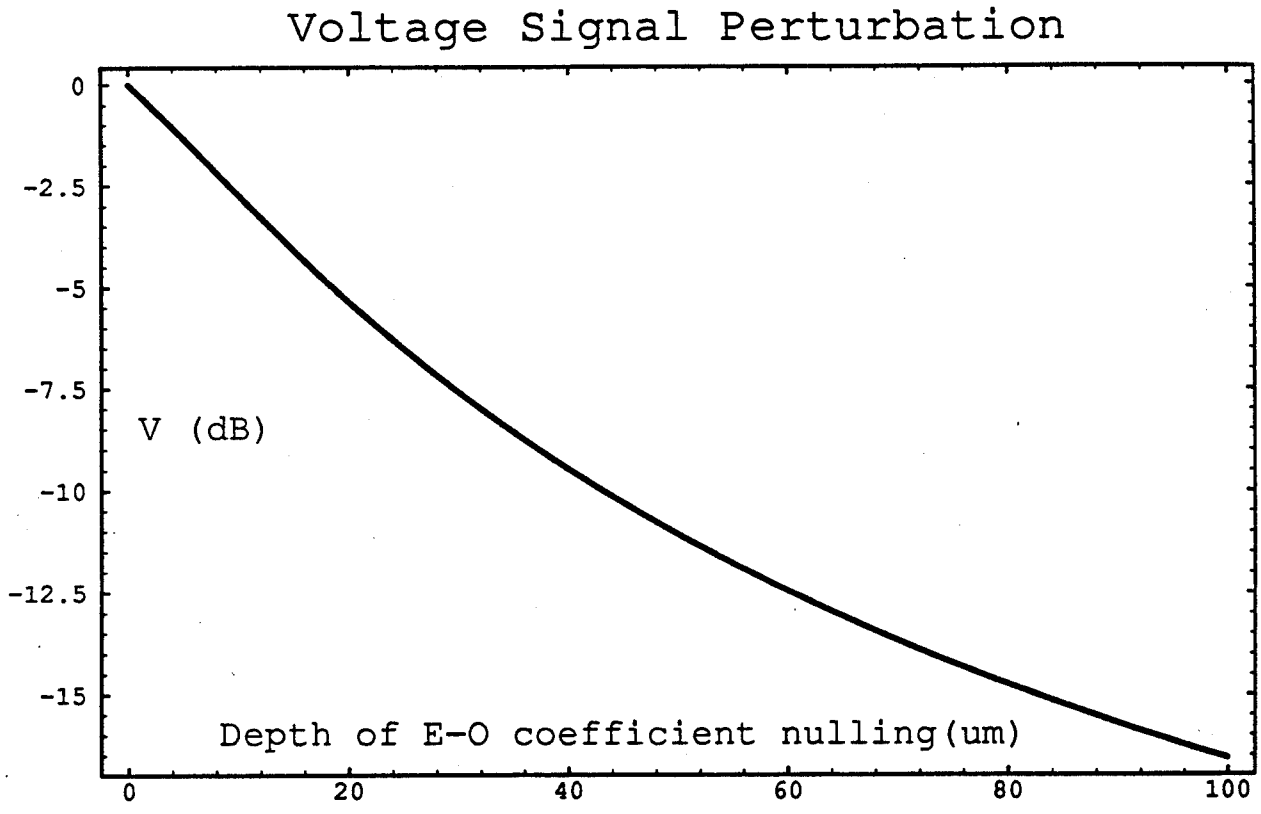
Voltage Signal Perturbation
0
-2.5
-5
-7.5
-10
-12.5
-15
V (dB)
Depth of E-O coefficient nulling(um)
0
20
40
60
80
100

Fig 11

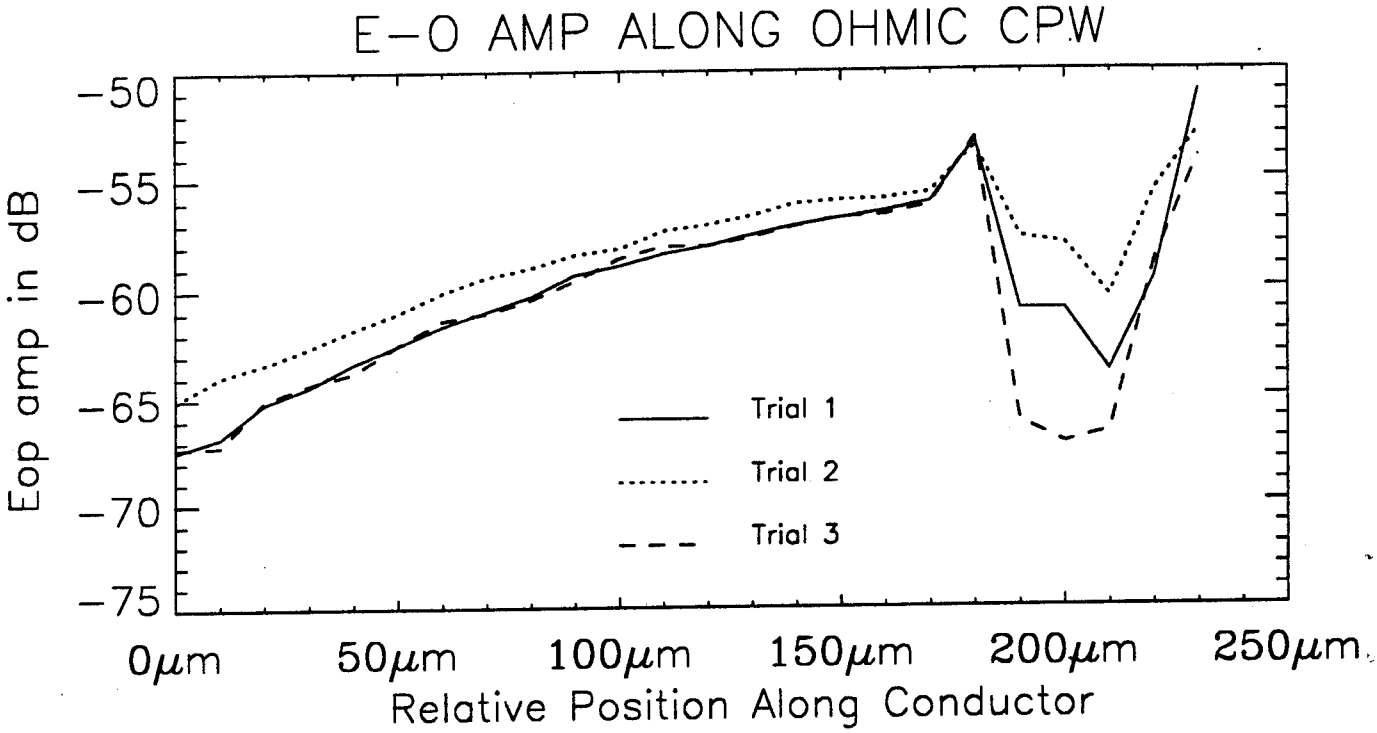
E–O AMP ALONG OHMIC CPW
Eop amp in dB
−50
−55
−60
−65
−70
−75
Trial 1
Trial 2
Trial 3
0μm
50μm
100μm
150μm
200μm
250μm
Relative Position Along Conductor

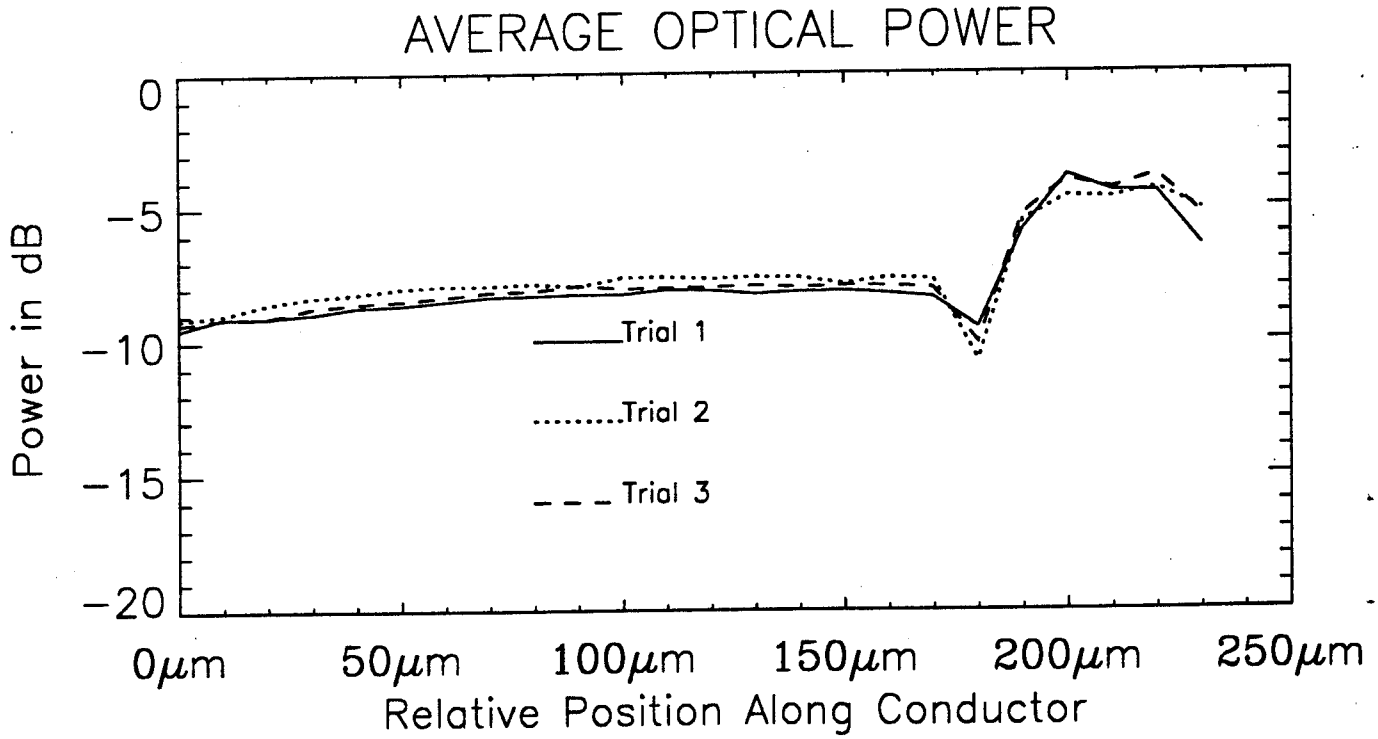
AVERAGE OPTICAL POWER
Power in dB
0
−5
−10
−15
−20
Trial 1
Trial 2
Trial 3
0μm
50μm
100μm
150μm
200μm
250μm
Relative Position Along Conductor

12(a) 12(b)

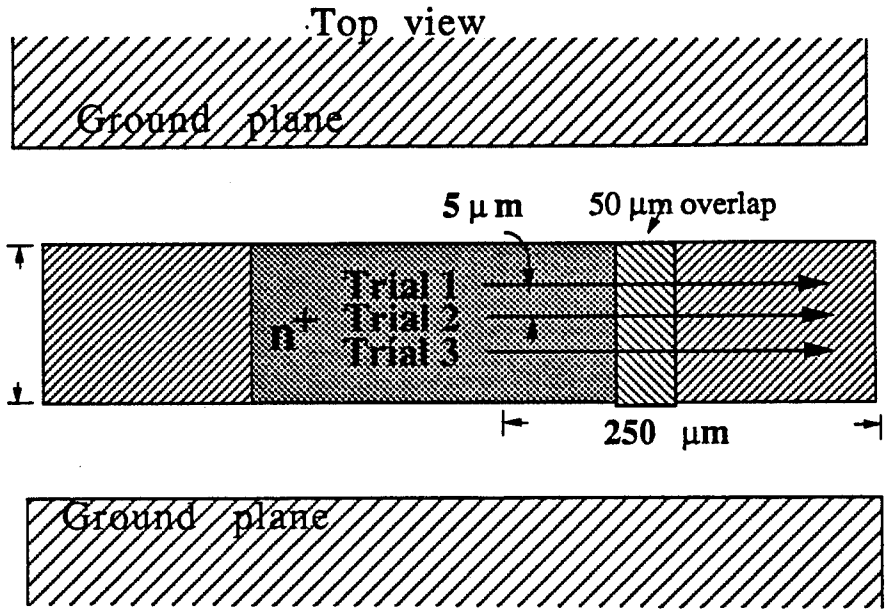
Top view
Ground plane
5 μm
50 μm overlap
Trial 1
Trial 2
Trial 3
n+
250 μm
Ground plane

Fig 12C

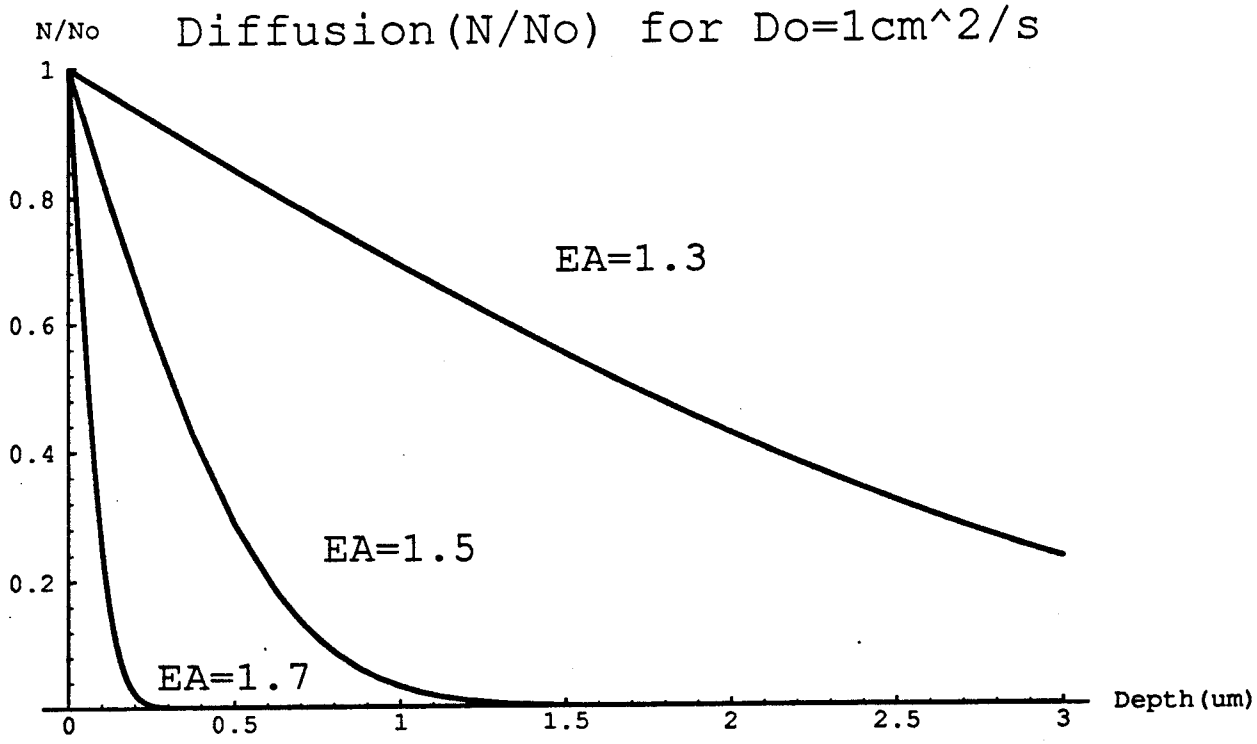
Diffusion(N/No) for Do=1cm^2/s
N/No
1
0.8
0.6
0.4
0.2
EA=1.3
EA=1.5
EA=1.7
0
0.5
1
1.5
2
2.5
3
Depth(um)

Fig 13 (9)

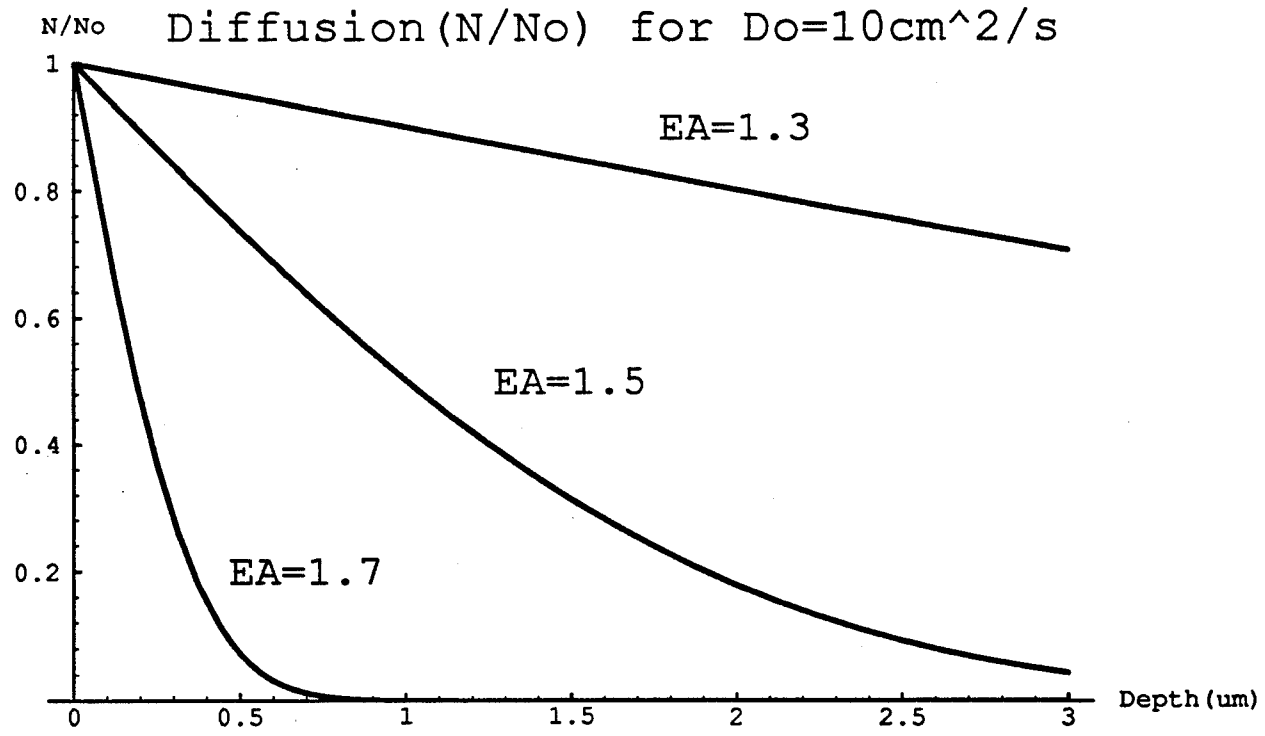
N/No
Diffusion(N/No) for Do=10cm^2/s
1
0.8
0.6
0.4
0.2
EA=1.3
EA=1.5
EA=1.7
0
0.5
1
1.5
2
2.5
3
Depth(um)

Fig 13 (b)

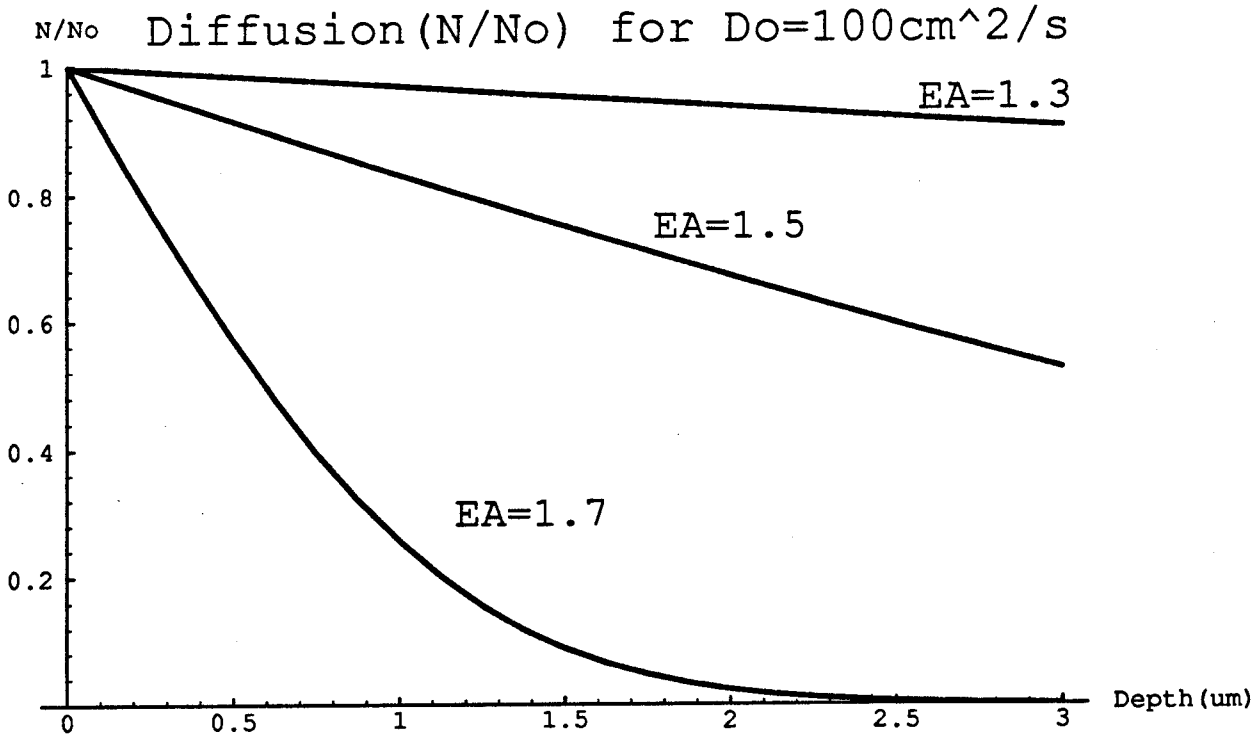
N/No
Diffusion(N/No) for Do=100cm^2/s
1
0.8
0.6
0.4
0.2
EA=1.3
EA=1.5
EA=1.7
0
0.5
1
1.5
2
2.5
3
Depth(um)

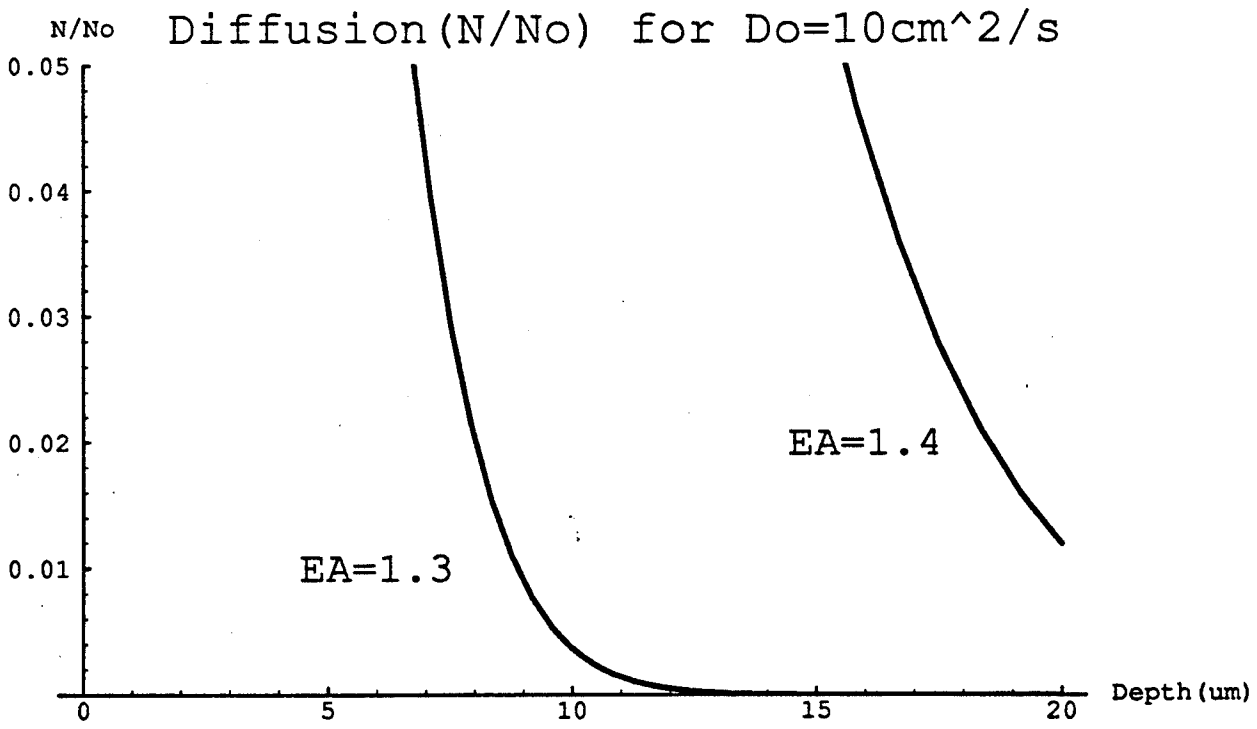
N/No
Diffusion(N/No) for Do=10cm^2/s
0.05
0.04
0.03
0.02
0.01
EA=1.4
EA=1.3
0
5
10
15
20
Depth (um)

Fig 14